Application of modified modal theory in the modelling of practical transformers

D.J. Wilcox
W.G. Hurley
T.P. McHale
M. Conlon

Indexing terms: Transformers, Modal theory, Electromagnetic transients

Abstract: The paper is concerned with validating a new form of transformer model aimed at efficient and accurate representation of power transformers in the calculation of electromagnetic transients arising under service and test conditions, where the duration of interest may be as short as tens of microseconds or as long as 5 ms or more. The principal concern is to confirm that modal models, based on a modified theory of modal analysis, retain their efficient structure when proper account is taken of the effects of transient-flux penetration into a practical core, and consequent frequency dependence of inductive and resistive parameters. This is done by modelling representative test windings on a commercial laminated core and comparing computed results with test results.

1 Introduction

A new form of transformer model, aimed at efficient and accurate representation of power transformers under general transient conditions, has been proposed in a companion paper [1]. The advantage of the structure of this form of model is that it offers opportunities for very large reductions in computational requirements compared with modelling on the basis of direct circuit analysis [2]. However, to realise the gains in full, it is essential that the transformation and distribution matrixes of the modal model may be treated as purely real and completely independent of frequency.

In the companion paper it was shown that these matrixes are always real and completely independent of frequency in the idealised case of lossless transformers with frequency-independent parameters. The present paper investigates the extent to which this remains the case in relation to practical transformers and also demonstrates the nature of practical models.

To this end, the authors have modelled the behaviour of test windings on a commercial 25 kVA core. Whilst this core is small, it manifests all the essential characteristics of transformer cores in general. In particular, the induction of eddy currents in the core gives rise to a complex loss mechanism and, more significantly, to a frequency dependence of all inductive couplings. There seems little, if any, reason to suppose that these phenomenological effects are any less severe in a small transformer than in a larger transformer.

Paper 9059C (P7), first received 13th September 1991 and in revised form 28th April 1992

Prof. Wilcox, Dr. Hurley and Mr. McHale are with the Faculty of Engineering, University College, Galway, Republic of Ireland

Dr. Conlon is with the Department of Electrical and Computer Systems Engineering, Monash University, Clayton, Victoria 3168, Australia

2 The test windings

Fig. 1 shows the topography of 16 disks which were wound onto one of the outer limbs of a commercial 25 kVA core. Each disk has six turns of heavy strip. The two ends of each disk are brought out to terminals on a terminal board for connection either as a single winding (eight disks of 12 turns) or as two windings (an inner winding of eight six-turn disks and an outer winding of eight six-turn disks). Details of the core are given in Appendix 8.1.

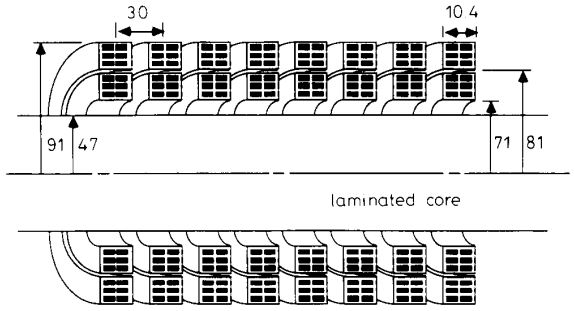

Fig. 1 *Test windings on the 25 kVA core (dimensions in mm)*

The natural capacitances of the configuration (Fig. 1) turn out to be rather low, resulting in much higher natural resonant frequencies than would occur in large transformers. To bring behaviour into line with conditions obtaining in large transformers, external capacitances have been introduced. The external capacitance network for the case where the disks are connected as a single winding is shown in Fig. 2. The external capacitance network for the case where the disks form two

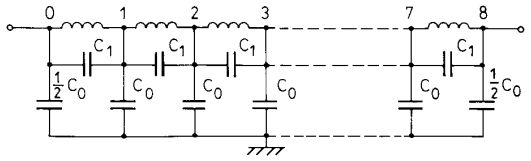

Fig. 2 *Externally connected capacitance network for single-winding configuration*

windings is shown in Fig. 3. Capacitance values are given in Appendix 8.2. In both cases, the introduced capacitances swamp the natural capacitances and bring the dominant natural frequencies down into the range typical of large transformers (i.e. ~20 kHz to ~200 kHz).

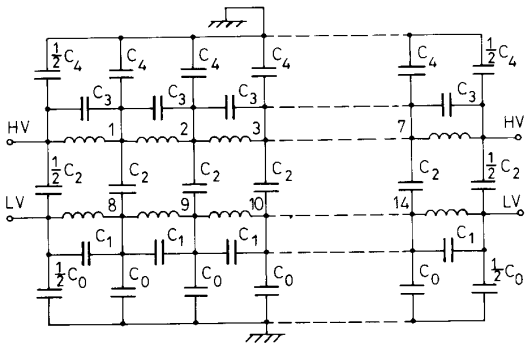

Fig. 3 *Externally connected capacitance network for 2-winding configuration*

Accurate modelling of the system of coils shown in Fig. 1, whether connected as in Fig. 2 or as in Fig. 3, calls for accurate account of the role played by the induction of eddy currents into the core. At high frequencies, eddy currents largely inhibit flux penetration into the core and inductive couplings are relatively weak (especially between remote coils). As the frequency reduces, the couplings become stronger until, eventually, a limiting condition is reached where there is total flux penetration into the core. The inductive couplings are thus quite strongly frequency dependent and this frequency dependence must be taken into account if the behaviour of the model is to match that of its physical couterpart.

The frequency dependence is taken into account in modelling the present test windings by employing a new impedance formula [4]. This formula not only accounts for the frequency dependence of the inductive couplings but also accounts for damping effects caused by the eddy currents. It is noteworthy that the formula only calls for the topographical data given in Fig. 1 and the core data given in Appendix 8.1. It is necessary, however, to correct a typographical error in Reference 4. Eqn. 11 of Reference 4 should read

$$F_1(\beta_n b) = \mu_0 \left\{ \frac{f(\beta_n b) - (\mu_0/\mu_z) f(\Gamma_n b)}{g(\beta_n b) + (\mu_0/\mu_z) f(\Gamma_n b)} \right\} \tag{1}$$

It is also necessary to account for the impedance of the copper strip of the windings, as this also affects damping. This is done, when forming the modal model, by supplementing each self impedance term, i.e. each term of the form $Z_{ii}(k, k)$, with the term $z_i(k)$ given by

$$z_i(k) = R_{DC}(i, k) + \frac{x_i(k)}{g_i(k)} \sqrt{\left(\frac{s\mu_0}{\sigma}\right)} \tag{2}$$

where $R_{DC}(i, k)$ is the DC resistance of the kth coil of the ith winding, $g_i(k)$ is the effective girth of the wire and $x_i(k)$ is its length. Values for these parameters are given in Appendix 8.3. $\mu_0 = 4\pi \times 10^{-7}$ (the permeability of free space) and $\sigma = 5.81 \times 10^7$ (the conductivity of the copper wire).

3 Modal model of the single-winding configuration

This Section discusses the nature of the component matrixes of the modal model (Fig. 4) for the single-winding configuration. These matrices were calculated as detailed in Reference 1 using given data. The objective is to show that the essential features of the modal model are largely the same as those established [1] for lossless transformers with frequency-independent parameters and to clarify the nature of differences where they arise.

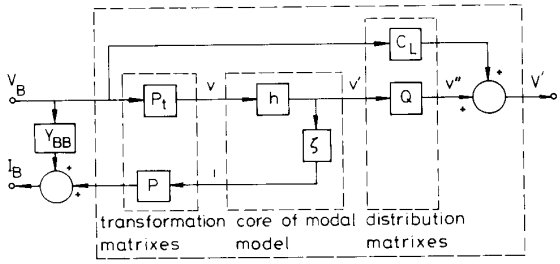

Fig. 4 *Structure of the modal model*

3.1 Modal-transformation matrix P_t

The modal-transformation matrix P_t transforms the boundary voltages into modal voltages. For lossless transformers with frequency-independent parameters, it was found that P_t was real and independent of frequency. To retain the computational advantages of the modal structure, it is desired that P_t may also be taken as real and independent of frequency in practical cases.

In the present practical case, it turns out (as expected) that P_t is neither real nor independent of frequency. It is not practical to give a complete set of results for the range from 100 Hz to 1 MHz. The following results are, however, representative

P_t(10 kHz)

$$= \begin{bmatrix} 0.6225 - j0.0014 & 0.6225 - j0.0014 \\ 0.1262 + j0.0013 & -0.1262 - j0.0013 \\ 0.0551 + j0.0025 & 0.0551 + j0.0025 \\ 0.0205 + j0.0007 & -0.0205 - j0.0007 \\ 0.0134 + j0.0008 & 0.0134 + j0.0008 \\ 0.0056 + j0.0002 & -0.0056 - j0.0002 \\ 0.0031 + j0.0002 & 0.0031 + j0.0002 \end{bmatrix}$$

P_t(100 kHz)

$$= \begin{bmatrix} 0.6225 - j0.0013 & 0.6225 - j0.0013 \\ 0.1310 + j0.0042 & -0.1310 - j0.0042 \\ 0.0552 + j0.0023 & 0.0552 + j0.0023 \\ 0.0214 + j0.0013 & -0.0214 - j0.0013 \\ 0.0135 + j0.0007 & 0.0135 + j0.0007 \\ 0.0058 + j0.0004 & -0.0058 - j0.0004 \\ 0.0032 + j0.0002 & 0.0032 + j0.0002 \end{bmatrix}$$

Thus whilst P_t is not strictly real or independent of frequency, it is nearly so (in fact remarkably so, given that account has been taken of frequency-dependent parameters and losses). The modal model (in its efficient form) treats P_t as purely real and independent of frequency. In the present case it is taken to be given by

$$P_t = \begin{bmatrix} 0.62248 & 0.62248 \\ 0.12804 & -0.12804 \\ 0.05522 & 0.05522 \\ 0.02107 & -0.02107 \\ 0.01347 & 0.01347 \\ 0.00577 & -0.00577 \\ 0.00316 & 0.00316 \end{bmatrix} \tag{3}$$

In this approximation, the kth row has been chosen as the real part of the kth row of $\boldsymbol{P}_t(j\omega_k)$, i.e. the real part of the kth row of $\boldsymbol{P}_t$ when calculated at the kth resonant frequency (the resonant frequencies are identified in the next Section). The validity of this approximation is confirmed later.

3.2 Modal transfer functions

The nature of the seven modal transfer functions (the elements of the diagonal matrix $\boldsymbol{h}$ in the modal model) is exemplified by $h_1(s)$ (the modal transfer function for mode 1). The amplitude spectrum of $h_1(s)$ is shown by the full line in Fig. 5. Its character is identified as similar to that of a transfer function of the form

$$h'_k(s) = \frac{-s(s + 2\delta_k \omega_k)}{s^2 + 2\delta_k \omega_k s + \omega_k^2} \tag{4}$$

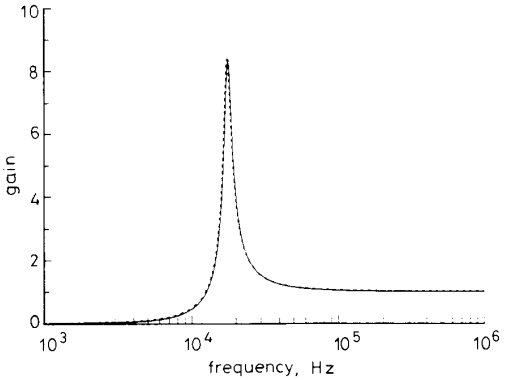

Fig. 5 *Amplitude spectrum of the transfer function for mode 1*
——— calculated frequency response $|h_1(j\omega)|$
------- approximated frequency response $|h'_1(j\omega)|$

This is confirmed by the broken line in Fig. 5 which shows the spectrum of $h'_1(s)$ as calculated using the parameters given in the first row of Table 1. These parameters were obtained by a least-squares fit of $h'_1(s)$ to $h_1(s)$. Results for the other modes were similar, a good fit being obtained in each case using the parameters given in Table 1.

The nature of the modal transfer functions of the model is thus consistent with that established in the companion work for lossless transformers with frequency-independent parameters. In particular, each modal transfer function has an associated natural resonant frequency. The main difference is that, on account of losses, resonant peaks are now damped. The extent of the damping associated with each modal transfer function is indicated, as a damping ratio, in Table 1.

Table 1: Parameters of the modal transfer functions

Mode k	Resonant frequency		Damping ratio
	f_k (kHz)	ω_k (rad/s)	δ_k
1	17.69	1.112×10^5	0.0597
2	32.21	2.024×10^5	0.0292
3	44.39	2.789×10^5	0.0221
4	53.26	3.346×10^5	0.0216
5	60.52	3.802×10^5	0.0225
6	65.66	4.125×10^5	0.0236
7	68.95	4.332×10^5	0.0244

Whilst eqn. 4 has been useful, as an approximation, in clarifying the nature of the modal transfer functions, it is not needed as part of the present frequency-domain model. Instead, the $h_k(s)$ are computed directly as numerical values at sample values of s, consistent with implementation of the numerical-Laplace-transform technique [5]. Approximations of the sort indicated in eqn. 4 will be considered in later work, notably in connection with the development of time-domain models.

3.3 Modal transfer admittances

The modal transfer admittances are the elements of the diagonal matrix ζ in the modal model. In frequency-domain models (the concern of the present work), these elements are simply computed and stored at appropriate sample values of s. The fact that the elements turn out to be purely capacitive in nature will, however, be exploited in future work concerned with the development of time-domain models.

3.4 Modal distribution matrix $\boldsymbol{Q}$

For lossless transformers with frequency-independent parameters, $\boldsymbol{Q}$ was found to be purely real and independent of frequency. To be able to exploit fully the computational advantages of the modal method, it is required that $\boldsymbol{Q}$ may also be taken as real and independent of frequency in practical cases. For the present practical case, the results given in Tables 2 and 3 are representative of results within the range 100 Hz to 1 MHz. To a very large extent, more so even than in the case of $\boldsymbol{P}_t$, $\boldsymbol{Q}$ is real and independent of frequency. The modal model (in its efficient form) treats it as purely real and completely independent of frequency as given by

$$\boldsymbol{Q} = \begin{bmatrix} 0.1780 & 0.3412 & 0.4635 & 0.5129 & 0.4970 & 0.3809 & 0.2154 \\ 0.3472 & 0.5024 & 0.4021 & 0.0420 & -0.3032 & -0.4862 & -0.3500 \\ 0.4668 & 0.3622 & -0.1381 & -0.4850 & -0.1879 & 0.3443 & 0.4610 \\ 0.5098 & 0.0000 & -0.4573 & -0.0000 & 0.5016 & -0.0000 & -0.4872 \\ 0.4668 & -0.3622 & -0.1381 & 0.4850 & -0.1879 & -0.3443 & 0.4610 \\ 0.3472 & -0.5024 & 0.4021 & -0.0420 & -0.3032 & 0.4862 & -0.3500 \\ 0.1780 & -0.3412 & 0.4635 & -0.5129 & 0.4970 & -0.3809 & 0.2154 \end{bmatrix} \tag{5}$$

where the kth column was chosen as the real part of the kth column of $\boldsymbol{Q}(j\omega)$ when calculated at the kth resonant frequency. The validity of this approximation is confirmed later.

The columns of $\boldsymbol{Q}$ (eqn. 5) distribute modal oscillations to the internal nodes of the winding. For example, the first column distributes mode-1 oscillations to the seven internal nodes of Fig. 2. The nature of the distributions is evident from Fig. 6 which shows the distributions for the illustrative cases of modes 1, 2 and 3. Dots correspond to numerical values taken from $\boldsymbol{Q}$. Evidently, the distributions are quasisinusoidal, as expected from classical theory. Note that each mode is formally identified by its spatial distribution (the spatial distribution of each mode being quite distinct from the spatial distributions of all the other modes).

Computational note: Since $\boldsymbol{Q}$ is an eigenvector matrix (obtained by diagonalisation of $\boldsymbol{D}$), there is no guarantee

Table 2: Columns of Q at 10 kHz

0.1780 − j0.0024	0.3416 − j0.0023	0.4635 + j0.0005	0.5122 + j0.0028	0.4969 + j0.0048	0.3799 + j0.0036	0.2153 + j0.0027
0.3472 − j0.0012	0.5023 + j0.0004	0.4020 + j0.0074	0.0403 + j0.0071	−0.3035 + j0.0074	−0.4868 + j0.0025	−0.3500 + j0.0012
0.4667 + j0.0008	0.3620 + j0.0017	−0.1384 + j0.0093	−0.4859 + j0.0035	−0.1879 + j0.0023	0.3445 − j0.0005	0.4609 + j0.0005
0.5097 + j0.0017	0.0000 + j0.0000	−0.4575 + j0.0085	0.0000 + j0.0000	0.5015 + j0.0012	−0.0000 + j0.0000	−0.4872 + j0.0018
0.4667 + j0.0008	−0.3620 − j0.0017	−0.1384 + j0.0093	0.4859 − j0.0035	−0.1879 + j0.0023	−0.3445 + j0.0005	0.4609 + j0.0005
0.3472 − j0.0012	−0.5023 − j0.0004	0.4020 + j0.0074	−0.0403 − j0.0071	−0.3035 + j0.0074	0.4868 − j0.0025	−0.3500 + j0.0012
0.1780 − j0.0024	−0.3416 + j0.0023	0.4635 + j0.0005	−0.5122 − j0.0028	0.4969 + j0.0048	−0.3799 − j0.0036	0.2153 + j0.0027

Table 3: Columns of Q at 100 kHz

0.1779 − j0.0021	0.3407 − j0.0026	0.4635 + j0.0006	0.5133 + j0.0031	0.4970 + j0.0041	0.3813 + j0.0039	0.2154 + j0.0023
0.3472 − j0.0010	0.5025 + j0.0004	0.4022 + j0.0066	0.0430 + j0.0077	−0.3032 + j0.0064	−0.4859 + j0.0027	−0.3500 + j0.0011
0.4668 + j0.0007	0.3626 + j0.0019	−0.1381 + j0.0084	−0.4846 + j0.0040	−0.1879 + j0.0022	0.3443 − j0.0004	0.4610 + j0.0005
0.5098 + j0.0015	0.0000 + j0.0000	−0.4573 + j0.0077	0.0000 + j0.0000	0.5016 + j0.0012	−0.0000 + j0.0000	−0.4872 + j0.0015
0.4668 + j0.0007	−0.3626 − j0.0019	−0.1381 + j0.0084	0.4846 − j0.0040	−0.1879 + j0.0022	−0.3443 + j0.0004	0.4610 + j0.0005
0.3472 − j0.0010	−0.5025 − j0.0004	0.4022 + j0.0066	−0.0430 − j0.0077	−0.3032 + j0.0064	0.4859 − j0.0027	−0.3500 + j0.0011
0.1779 − j0.0021	−0.3407 + j0.0026	0.4635 + j0.0006	−0.5133 − j0.0031	0.4970 + j0.0041	−0.3815 − j0.0039	0.2154 + j0.0023

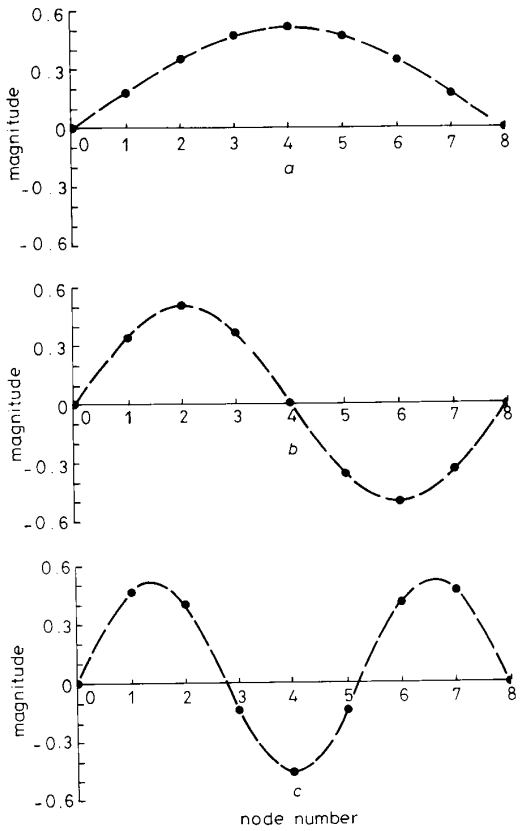

Fig. 6 *Modal distribution vectors*
a Mode 1
b Mode 2
c Mode 3

that the computation of Q using any practical algorithm (such as the power method) will necessarily arrange the columns of Q in the same order at all frequencies. It may not therefore be taken for granted that the first column of Q (as it emerges from the diagonalisation process) will always correspond to the same mode at all frequencies. A technique for ensuring that the columns of Q are always arranged in the same modal order, at all frequencies, is described in Appendix 8.4.

3.5 Distribution matrix C_L

The distribution matrix C_L gives the final, or low-frequency, distribution of the boundary voltages to the internal nodes of the winding. Theoretically, C_L is completely independent of frequency for lossless transformers with frequency-independent parameters. In practice, relative to the present test winding, it is found to be largely independent of frequency — converging to the true final distribution as the frequency tends to zero. In the model, it is taken to be the real part of the distribution matrix at 100 Hz, i.e.

$$C_L = \begin{bmatrix} 0.8757 & 0.1243 \\ 0.7508 & 0.2492 \\ 0.6255 & 0.3745 \\ 0.5000 & 0.5000 \\ 0.3745 & 0.6255 \\ 0.2492 & 0.7508 \\ 0.1243 & 0.8757 \end{bmatrix} \quad (6)$$

The first column gives the distribution (relative to unit input) when the remote end of the winding is short-circuited whilst the second gives the distribution when the local end is short-circuited. Evidently these (quasifinal) distributions are very close to those expected for a uniform winding (which is the present case).

4.6 Admittance matrix Y_{BB}

The admittance matrix Y_{BB} (given by eqn. 18 of the companion paper) is independent of the process of modal decomposition and lies outside the main structure of Fig. 4. In the present frequency-domain model there is no requirement to establish its nature. It is simply calculated, as a frequency-dependent 2 × 2 matrix, at required sample values of s.

4 Transient results for the single-winding configuration

Fig. 7 shows the unit step response, half way down the winding (node 4), predicted by the modal model for the

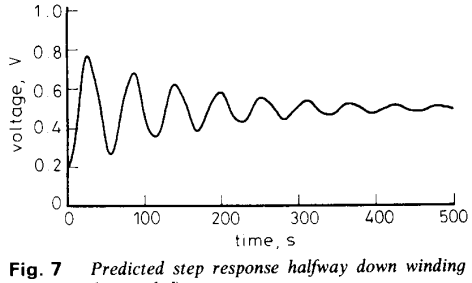

Fig. 7 *Predicted step response halfway down winding (modal model) (remote end grounded)*

case where the remote-end terminal (node 8) is grounded. For these results, P_t, Q and C_L were taken to be purely real and independent of frequency (as specified by eqns. 3, 5 and 6, respectively). Fig. 8 shows the result obtained without approximations, i.e. Fig. 8 gives the result corres-

ponding to direct circuit analysis. Evidently, to all practical purposes, the results are identical, helping to confirm that the transformation and distribution matrices may be taken as purely real and independent of frequency with negligible effect on accuracy.

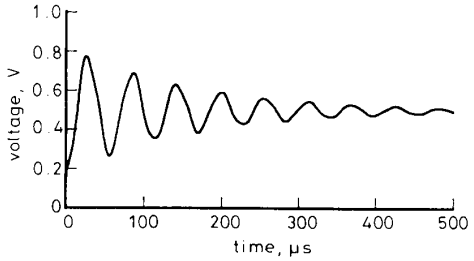

Fig. 8 *Predicted step response halfway down winding (exact solution) (remote end grounded)*

Fig. 9 shows the oscillographic record of the actual response. The degree of agreement is remarkable, and all the more remarkable for the fact that the model was constructed entirely from drawing-board data and physical constants. In particular, the model has predicted the correct overshoot and the correct degree of damping.

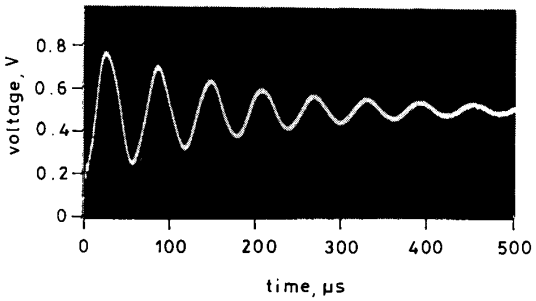

Fig. 9 *Measured step response halfway down winding (remote end grounded)*

Fig. 10 shows the step response, again half way down the winding (node 4), as predicted by the modal model for the very different case where the remote-end terminal

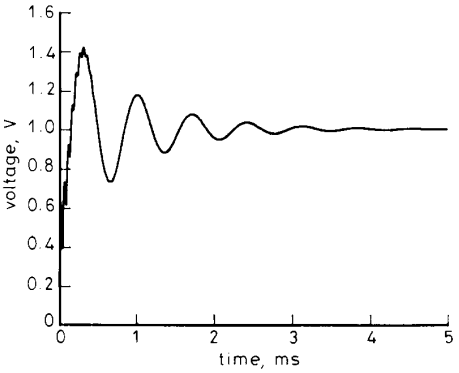

Fig. 10 *Predicted step response halfway down winding (remote end open circuit)*

(node 8) is open circuit. Fig. 11 shows the actual response. Again, the degree of agreement is remarkable. It is particularly important to note that the dominant resonant frequency when the winding is open circuit is quite different from when it was short-circuited (the time scales of Fig. 9 and 11 are not the same). The same model has thus performed equally well in the two contrasting cases (classical analysis called for separate models for the two cases).

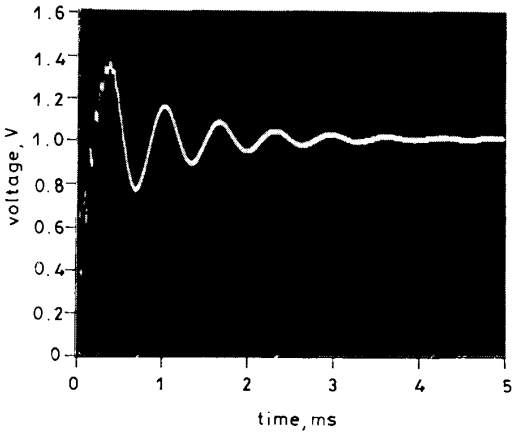

Fig. 11 *Measured step response halfway down winding (remote end open circuit)*

These results demonstrate, at least in a particular case, that $\boldsymbol{P}_t$, $\boldsymbol{Q}$ and $\boldsymbol{C}_L$ may be approximated as purely real and independent of frequency in the modelling of single-winding configurations.

5 Transient results for the 2-winding configuration

Modified modal theory was used, as described in the companion paper, to form a modal model for the 2-winding configuration using given data. The matrixes $\boldsymbol{P}_t$, $\boldsymbol{Q}$ and $\boldsymbol{C}_L$ (which turn out to be nearly real and almost independent of frequency) are taken to be purely real and independent of frequency in the model and are specified in Appendix 8.5. The validity of this approximation is evidenced by the following comparative results.

Fig. 12*a* shows the predicted transient response halfway down the primary winding (node 4 in Fig. 3) for the case of a unit step applied at local end of the high-voltage winding (all other terminals in Fig. 3 being open). This is evidently in good agreement with the measured result of Fig. 12*b*.

Results for the very different case where both ends of the secondary winding are short-circuited (the remote end of the high-voltage winding remaining open) are shown in Fig. 13. Other results, representative of the permutations of possibilities, are shown in Figs. 14 and 15. In all cases, the unit step is applied at the local end of the high-voltage winding. Fig. 15 relates to a case of surge transfer (from high to low voltage).

6 Conclusions

The paper has demonstrated the nature of a modal transformer model in a practical case. It has been shown, at least for the configurations considered, that the character of a modal transformer model remains essentially unchanged from that established in the companion work for lossless transformers with frequency-independent parameters when practical losses and frequency dependencies are taken into account. In particular, the modal transfer functions at the core of a modal model retain a simple resonant nature (but now damped on account of losses).

It has been particularly important to have shown, albeit only for particular test windings on a particular

core, that the transformation and distribution matrices remain, for all practical purposes, purely real and independent of frequency in spite of taking accurate account of frequency-dependent parameters and losses. The importance of having real and frequency-independent transformation and distribution matrices is that it confines all frequency dependence to the core of the model. This, and the fact that the n modal networks at the core of the modal model are completely decoupled from one another, vastly reduce computational requirements, by a factor of the order of n^2, compared with direct application of circuit-analysis methods (where n is the number of internal nodes in the original lumped-parameter transformer representation).

Since a reasonably detailed representation of a power transformer (including high-, medium- and low-voltage

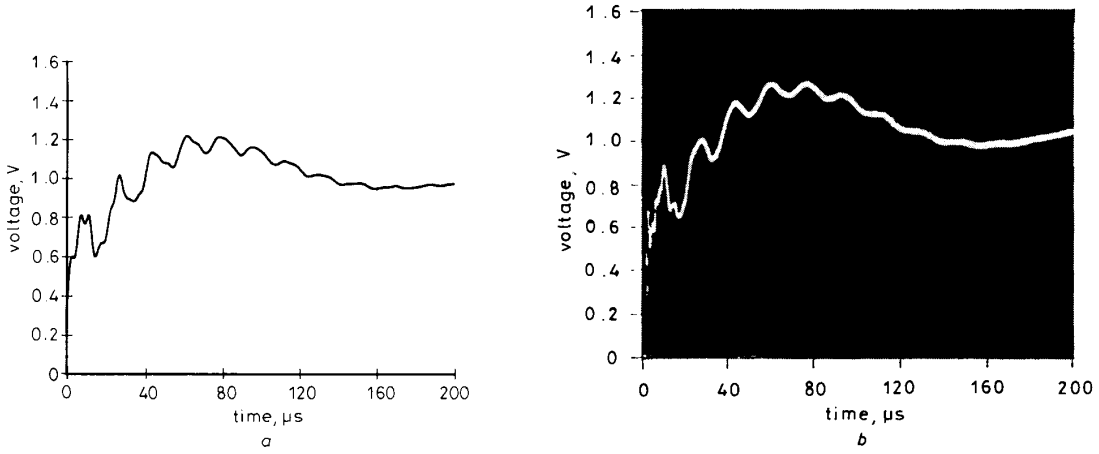

Fig. 12 *Step response halfway down primary winding (all terminals open)*
a Predicted *b* Measured

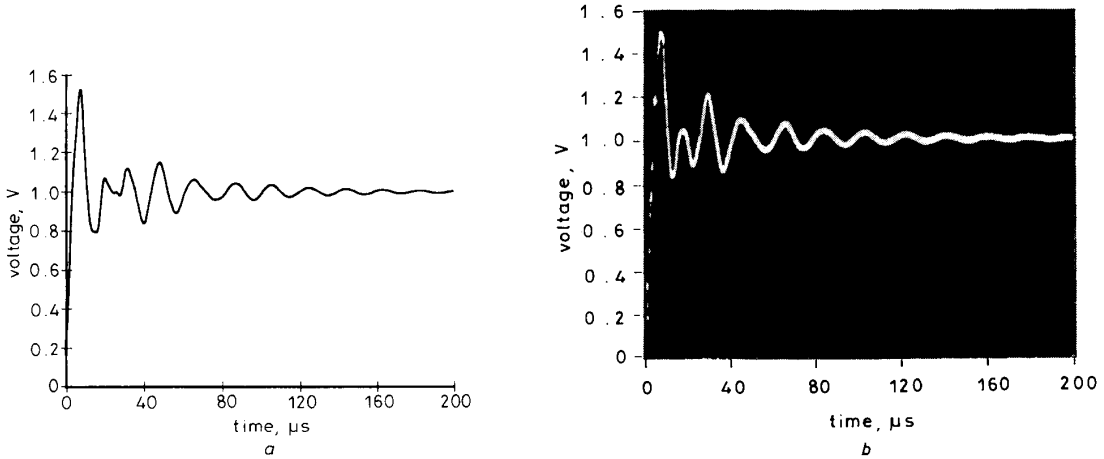

Fig. 13 *Step response halfway down primary winding (low-voltage winding grounded at both ends)*
a Predicted *b* Measured

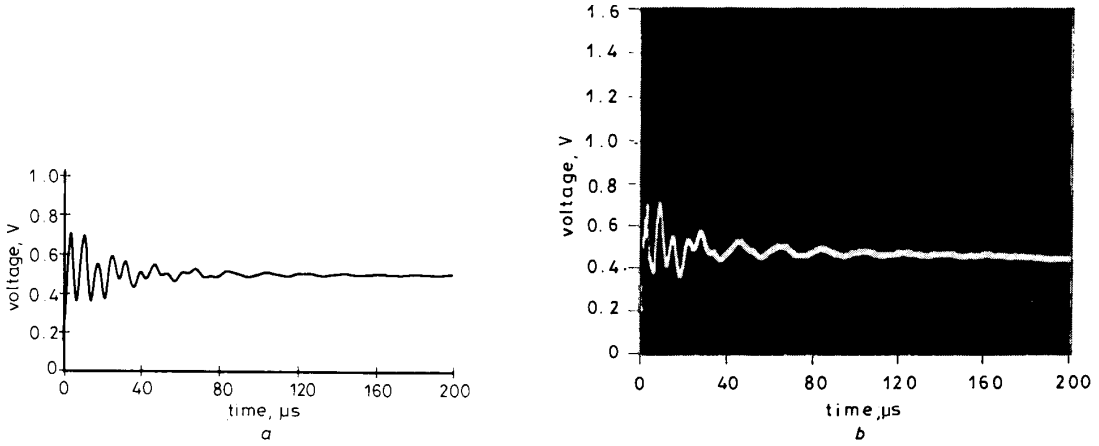

Fig. 14 *Step response halfway down primary winding (all terminals grounded except excited terminal)*
a Predicted *b* Measured

and tapping windings) would require n to be at least 28, the computational savings in prospect are very large, possibly reducing a computation time of many minutes

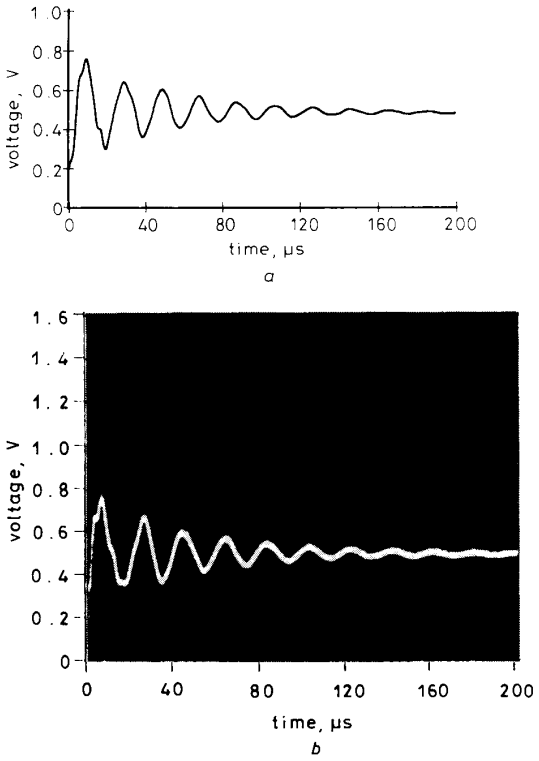

Fig. 15 *Step response halfway down low-voltage winding (all remote terminals grounded)*
a Predicted
b Measured

to under 1 s (excluding the once-off computation time required to set up the modal model). This makes it possible to envisage including accurate transformer models in the calculation of electromagnetic transients in power networks (especially when interest centres on whether a particular transformer would be vulnerable to internal damage under specified transient conditions).

As an important side issue, the paper has shown that it is possible to obtain highly accurate predictions of internal transients on the basis of drawing-board data (in conjunction with certain physical constants). This success, which does not appear to have been achieved previously, owes itself very largely to the use of a new impedance formula [4]. This formula takes accurate account of the dynamic process of transient flux penetration into a practical core. The accuracy involved is made apparent by the very close agreement between predicted transient waveshapes and experimental results.

Further work is in progress to convert the present frequency-domain model into a time-domain counterpart, with a view to eventual incorporation into the industry-standard EMTP transients program.

7 References

1 WILCOX, D.J., and McHALE, T.P.: 'Modified theory of modal analysis for the modelling of multiwinding transformers', *IEE Proc. C*, (companion paper)
2 DEGENEFF, R.C.: 'A general method for determining resonance in transformer windings', *IEEE Trans.*, 1977, **PAS-96**, (2), pp. 423–430
3 WILCOX, D.J.: 'Theory of transformer modelling using modal analysis', *IEE Proc. C, Gen. Trans. & Distrib.*, 1991, **138**, pp. 121–128
4 WILCOX, D.J., HURLEY, W.G., and CONLON, M.: 'Calculation of self and mutual impedances between sections of transformer windings', *IEE Proc. C, Gen. Trans. & Distrib.*, 1989, **136**, pp. 308–314
5 WILCOX, D.J.: 'Numerical Laplace transformation and inversion', *Int. J. Elect. Enging. Educ.*, 1978, **15**, pp. 247–265

8 Appendixes

8.1 Details of the core

The 25 kVA core, made from 'Unisil' 27M4 0.27 mm laminations, has the dimensions shown in Fig. 16. The core parameters were chosen as $\rho = 0.0103\ \Omega$m, $\alpha = 7 \times 10^{-7}$, $\mu_z(\text{rel}) = 843$, $\mu_r/\mu_z = 0.1$ and $\lambda(\text{eff}) = 0.976$ m, as determined experimentally (and defined) in Reference 4.

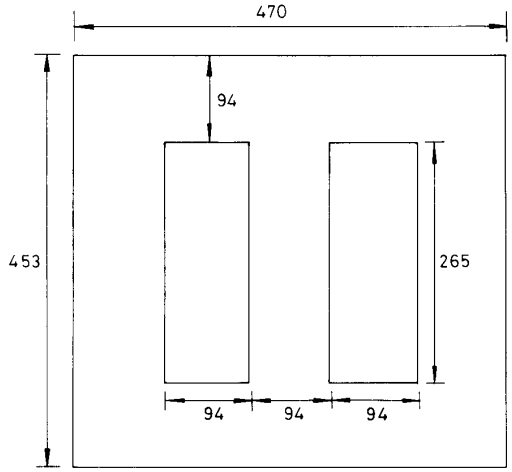

Fig. 16 *Dimensions of 25 kVA core, mm*

8.2 Capacitance values

For the single-winding configuration:

$C_0 = 0.050\ \mu$F

$C_1 = 0.328\ \mu$F

For the 2-winding configuration:

$C_0 = 0.01\ \mu$F

$C_1 = 0.1\ \mu$F

$C_2 = 0.02\ \mu$F

$C_3 = 0.1\ \mu$F

$C_4 = 0.005\ \mu$F

8.3 Details of coils

Single-winding configuration:

$x_1(k) = 6.107$ m $(k = 1, 2, \ldots, 8)$

$g_1(k) = 0.017$ m $(k = 1, 2, \ldots, 8)$

$R_{DC}(1, k) = 0.3\ \Omega^*$ $(k = 1, 2, \ldots, 8)$

2-winding configuration:

$x_1(k) = 3.242$ m $(k = 1, 2, \ldots, 8)$

$x_2(k) = 2.865$ m $(k = 1, 2, \ldots, 8)$

$g_1(k) = g_2(k) = 0.017$ m $(k = 1, 2, \ldots, 8)$

$R_{DC}(1, k) = 0.3\ \Omega^*$ $(k = 1, 2, \ldots, 8)$

$R_{DC}(2, k) = 0.3\ \Omega^*$ $(k = 1, 2, \ldots, 8)$

* inclusive of resistance of connections

8.4 Modal ordering technique

It has been shown, in Fig. 6, that the modal distribution vectors (the columns of $\boldsymbol{Q}$), are quasisinusoidal. It may also be confirmed that the columns of $\boldsymbol{Q}$ are quasi-orthogonal. The proposed method is based on this property. The first step is to calculate $\boldsymbol{Q}$ at some high frequency (e.g. 1 MHz) and define this as $\boldsymbol{Q}_H$. This establishes the modal order which is to be preserved at all other frequencies.

Each time $\boldsymbol{Q}$ is computed thereafter, by diagonalisation of $\boldsymbol{D}$, the matrix product $\boldsymbol{Q}_t\boldsymbol{Q}_H = \boldsymbol{M}$ is formed, where $\boldsymbol{Q}_t$ is the transpose of $\boldsymbol{Q}$. If $\boldsymbol{Q}$ has the same modal order as $\boldsymbol{Q}_H$ then $\boldsymbol{M}$ will approximate quite closely to a diagonal matrix (on account of intrinsic orthogonality). If not, then $\boldsymbol{M}$ will have the character of a diagonal matrix but with the columns rearranged. A search is made for the largest element in the first column of $\boldsymbol{M}$. If this is found to be in the kth position, then the first and kth columns of $\boldsymbol{Q}$ are interchanged (or unaltered if $k = 1$), with a corresponding interchange of the eigenvalues and of the rows of $\boldsymbol{Q}^{-1}$. Rows 1 and k of $\boldsymbol{M}$ are also interchanged, after which a search is made for the largest element in the second column of $\boldsymbol{M}$. If this is found to be in the mth position, then columns 2 and m of $\boldsymbol{Q}$ are interchanged (if $m \neq 2$), with corresponding reordering of the eigenvalues, reordering of the rows of $\boldsymbol{Q}^{-1}$ and finally reordering of the rows of $\boldsymbol{M}$. It is then a matter of finding the largest element in the third column of $\boldsymbol{M}$, and so on. The eventual modal order of $\boldsymbol{Q}$ will then be the same as that of $\boldsymbol{Q}_H$.

8.5 Transformation and distribution matrixes used in modal model of the 2-winding configuration

$$\boldsymbol{P}_t = \begin{bmatrix}
0.18281 & 0.39759 & 0.18281 & 0.39759 \\
0.02896 & 0.07709 & -0.02896 & -0.07709 \\
0.01962 & 0.02433 & 0.01962 & 0.02433 \\
0.65092 & -0.69564 & 0.65092 & -0.69564 \\
0.00602 & 0.01058 & -0.00602 & -0.01058 \\
0.00521 & 0.00506 & 0.00521 & 0.00506 \\
0.00175 & 0.00275 & -0.00175 & -0.00275 \\
0.00127 & 0.00111 & 0.00127 & 0.00111 \\
0.18869 & -0.20684 & -0.18869 & 0.20684 \\
0.07715 & -0.08592 & 0.07715 & -0.08592 \\
0.03860 & -0.04301 & -0.03860 & 0.04301 \\
0.02106 & -0.02370 & 0.02106 & -0.02370 \\
0.01156 & -0.01294 & -0.01156 & 0.01294 \\
0.00523 & -0.00591 & 0.00523 & -0.00591
\end{bmatrix}$$

$$\boldsymbol{C}_L = \begin{bmatrix}
0.8753 & 0.0004 & 0.1247 & -0.0004 \\
0.7504 & 0.0004 & 0.2496 & -0.0004 \\
0.6252 & 0.0002 & 0.3748 & -0.0002 \\
0.5000 & 0.0000 & 0.5000 & 0.0000 \\
0.3748 & -0.0002 & 0.6252 & 0.0002 \\
0.2496 & -0.0004 & 0.7504 & 0.0004 \\
0.1247 & -0.0004 & 0.8753 & 0.0004 \\
0.0003 & 0.8754 & -0.0003 & 0.1246 \\
0.0004 & 0.7504 & -0.0004 & 0.2496 \\
0.0002 & 0.6253 & -0.0002 & 0.3747 \\
0.0000 & 0.5000 & 0.0000 & 0.5000 \\
-0.0002 & 0.3747 & 0.0002 & 0.6253 \\
-0.0004 & 0.2496 & 0.0004 & 0.7404 \\
-0.0003 & 0.1246 & 0.0003 & 0.8754
\end{bmatrix}$$

$$\boldsymbol{Q} = \begin{bmatrix}
0.1248 & 0.2420 & 0.3383 & 0.1431 & 0.3759 & 0.3693 & 0.2825 & 0.1613 & 0.2482 & 0.3190 & 0.3497 & 0.3295 & 0.2578 & 0.1425 \\
0.2439 & 0.3568 & 0.2993 & 0.2761 & 0.0324 & -0.2189 & -0.3624 & -0.2600 & 0.3660 & 0.2653 & 0.0288 & -0.2141 & -0.3250 & -0.2355 \\
0.3282 & 0.2575 & -0.0857 & 0.3676 & -0.3532 & -0.1316 & 0.2561 & 0.3469 & 0.2643 & -0.1203 & -0.3354 & -0.1360 & 0.2275 & 0.3034 \\
0.3586 & 0.0000 & -0.3141 & 0.4000 & 0.0000 & 0.3775 & 0.0000 & -0.3619 & 0.0000 & -0.3456 & 0.0000 & 0.3333 & 0.0000 & -0.3253 \\
0.3282 & -0.2575 & -0.0857 & 0.3676 & 0.3532 & -0.1316 & -0.2561 & 0.3469 & -0.2643 & -0.1203 & 0.3354 & -0.1360 & -0.2275 & 0.3034 \\
0.2439 & -0.3568 & 0.2993 & 0.2761 & -0.0324 & -0.2189 & 0.3624 & -0.2600 & -0.3660 & 0.2653 & -0.0288 & -0.2141 & 0.3250 & -0.2355 \\
0.1248 & -0.2420 & 0.3383 & 0.1431 & -0.3759 & 0.3693 & -0.2825 & 0.1613 & -0.2482 & 0.3190 & -0.3497 & 0.3295 & -0.2578 & 0.1425 \\
0.1263 & 0.2401 & 0.3235 & -0.1135 & 0.3525 & 0.3379 & 0.2569 & 0.1440 & -0.2314 & -0.3226 & -0.3691 & -0.3584 & -0.2851 & -0.1598 \\
0.2467 & 0.3536 & 0.2838 & -0.2157 & 0.0319 & -0.1999 & -0.3222 & -0.2308 & -0.3451 & -0.2704 & -0.0302 & 0.2341 & 0.3618 & 0.2651 \\
0.3321 & 0.2552 & -0.0867 & -0.2847 & -0.3282 & -0.1224 & 0.2315 & 0.3074 & -0.2490 & 0.1218 & 0.3567 & 0.1482 & -0.2529 & -0.3414 \\
0.3629 & 0.0000 & -0.3060 & -0.3090 & 0.0000 & 0.3408 & 0.0000 & -0.3226 & 0.0000 & 0.3512 & 0.0000 & -0.3645 & 0.0000 & 0.3658 \\
0.3321 & -0.2552 & -0.0867 & -0.2847 & 0.3282 & -0.1224 & -0.2315 & 0.3074 & 0.2490 & 0.1218 & -0.3567 & 0.1482 & 0.2529 & -0.3414 \\
0.2467 & -0.3536 & 0.2838 & -0.2157 & -0.0319 & -0.1999 & 0.3222 & -0.2308 & 0.3451 & -0.2704 & 0.0302 & 0.2341 & -0.3618 & 0.2651 \\
0.1263 & -0.2401 & 0.3235 & -0.1135 & -0.3525 & 0.3379 & -0.2569 & 0.1440 & 0.2314 & -0.3226 & 0.3691 & -0.3584 & 0.2851 & -0.1598
\end{bmatrix}$$